Proceedings of the 18th International Conference on Nuclear Engineering
ICONE18
May 17-21, 2010, Xi'an, China

ICONE18-30188

NUMERICAL STUDY ON PASSIVE CONTROL OF THERMAL STRIPING PHENOMENON USING LORENTZ FORCE IN FAST REACTOR

Takashi TAKATA
Graduate School of Engineering, Osaka University
2-1 Yamada, Suita, Osaka, 565-0871, Japan
Phone: +81-6-6879-7891 Fax: +81-6-6879-7891
Email : takata_t@see.eng.osaka-u.ac.jp

Takeshi FUKUDA
Graduate School of Engineering, Osaka University
2-1 Yamada, Suita, Osaka, 565-0871, Japan
Phone: +81-6-6879-4080 Fax: +81-6-6879-4080
Email : fukuda@ppl.eng.osaka-u.ac.jp

Akira YAMAGUCHI
Graduate School of Engineering, Osaka University
2-1 Yamada, Suita, Osaka, 565-0871, Japan
Phone: +81-6-6879-7890 Fax: +81-6-6879-7891
Email : yamaguchi@see.eng.osaka-u.ac.jp

Akihiro UCHIBORI
Japan Atomic Energy Agency
4002 Narita, O-arai, Ibaraki, 311-1393, Japan
Phone: +81-29-267-4141 Fax: +81-29-267-3675
Email: uchibori.akihiro@jaea.go.jp

Nobuyuki KIMURA
Japan Atomic Energy Agency
4002 Narita, O-arai, Ibaraki, 311-1393, Japan
Phone: +81-29-267-4141 Fax: +81-29-267-3675
Email: kimura.nobuyuki@jaea.go.jp

Hideki KAMIDE
Japan Atomic Energy Agency
4002 Narita, O-arai, Ibaraki, 311-1393, Japan
Phone: +81-29-267-4141 Fax: +81-29-267-3675
Email: kamide.hideki@jaea.go.jp

ABSTRACT

Liquid sodium, used as a coolant of fast reactor (FR), is an electromagnetic fluid. When a magnetic field is embedded to liquid sodium flow, the Lorentz force will be induced and flow structure such as a turbulent mixing phenomenon will be influenced. In a FR piping system, thermal fatigue is one of key issues that may occur after a piping junction of different fluid temperature.

In the present paper, a numerical study of sodium flow induced by the Lorentz force on a turbulent mixing after the junction has been carried out. The large eddy simulation (LES) coupled with the electromagnetic field analysis is used for this purpose. The governing equations of the electric density field and the magnetic flux density fields are solved separately so that the solenoidal condition is satisfied non-iteratively. The fractional step method is applied to the present coupling in the simulation.

As a result of the numerical investigation, it is demonstrated that the temperature fluctuation due to turbulent mixing weakens after it runs through the magnetic field caused by the Lorentz force and thus the thermal fatigue will be suppressed. Accordingly, it is concluded that the passive control of the thermal fatigue will be possible by adding a magnetic field.

NOMENCLATURE

$\boldsymbol{B}$	magnetic flux density vector
Cp	specific heat
Cs	Smagorinsky constant (=0.1)
$\mathbf{D}$	electric flux density vector
D_b	side length of branch duct
D_m	side length of main duct
F_L	Lorentz force vector per unit volume
$\mathbf{g}$	gravity vector
$\mathbf{H}$	magnetic field intensity vector
Ha	Hartmann number

h	enthalpy
$\mathbf{j}$	current density vector
Pr_t	turbulent Prandtl number
p	pressure
Q_J	Joule heat per unit volume
Re	Reynolds number
T	temperature
t	time
$\mathbf{u}$	velocity vector
U_m	average velocity of main duct
x_k	k-th coordinate
(Symbol)	
β	Hall constant
ΔT	temperature difference between main and branch ducts
Δt	time step of computation
λ	thermal conductivity
μ	molecular viscosity
μ_m	magnetic permeability
ν_t	SGS eddy viscosity
ρ	density
σ	electric conductivity
$\otimes$	cross product
(Superscript)	
n	current time step
$\bar{\cdot}$	ensemble average of SGS

INTRODUCTION

In a fast reactor (FR), liquid sodium is used as a coolant material because of its excellent characteristics of heat transport capability and neutron degradation. On the other hand, liquid sodium is invisible fluid and thus a development of flow field measurement technique is a challenge. Fukuda et al. (2010) have been developing a direct observation method of liquid sodium flow using vacuum ultra violet (VUV) radiation.

Liquid sodium is also an electromagnetic fluid and the Lorentz force will be induced and flow structure, ex. turbulent mixing, be influenced when magnetic field is embedded. In the direct observation of liquid sodium (Fukuda et al., 2010), it is also planned to investigate the influence of the Lorentz force on the flow structure.

Thermal fatigue is one of key issues in the fast reactor piping system, which is caused by temperature fluctuation due to turbulent mixing that occurs just after a pipe junction of different fluid temperatures (called thermal striping). For the purpose of reducing the temperature fluctuation, Nagao et al. (2004) have investigated the influence of the turbulence promoter. The turbulence promoter enhances the turbulent mixing resulting in a smaller fluctuation region.

The Lorentz force can affect the turbulent mixing phenomenon without any devices inside the pipe. On the contrary, the Lorentz force reduces turbulence in general. From the viewpoint of the structural integrity from the thermal fatigue, a temperature fluctuation of fluid near the structure is more important than a stationary temperature gradient along the structure surface. Besides, liquid sodium has a high thermal conductivity that leads a rapid thermal equilibrium. Hence, it is possible that the thermal fatigue is reduced by adding a magnetic field at a junction of pipe.

In the present paper, the influence of the Lorentz force on the thermal striping phenomenon has been investigated numerically. The large eddy simulation (LES) is applied as a turbulence model. As concerns the electromagnetic field analysis, the governing equations of the electric density and the magnetic flux density are solved separately to satisfy the solenoidal condition non-iteratively. The fractional step method is applied to the coupling between the thermal hydraulics and electromagnetic fields analyses.

NUMERICAL METHOD

In the thermal hydraulics simulation, the following governing equations are solved with the Simplified Maker and Cell method (SMAC).

[Mass]

$$\frac{\partial \bar{\rho}}{\partial t} + \nabla \cdot \bar{\rho}\bar{\mathbf{u}} = 0, \tag{1}$$

[Momentum]

$$\bar{\rho}\frac{\partial \bar{\mathbf{u}}}{\partial t} + \nabla \cdot \bar{\rho}\bar{\mathbf{u}}\bar{\mathbf{u}} = -\nabla \bar{p} + \frac{\partial}{\partial x_k}\left[(\bar{\mu} + \bar{\rho}\nu_t)\frac{\partial \bar{\mathbf{u}}}{\partial x_k}\right] + (\bar{\rho} - \rho_0)\mathbf{g} + \bar{\mathbf{F}}_L, \tag{2}$$

[Energy]

$$\frac{\partial \bar{\rho}\bar{h}}{\partial t} + \nabla \cdot \bar{\rho}\bar{h}\mathbf{u} = \frac{\partial}{\partial x_k}\left[(\bar{\lambda} + \bar{\rho}\overline{Cp}\frac{\nu_t}{Pr_t})\frac{\partial \bar{T}}{\partial x_k}\right] + \bar{Q}_J. \tag{3}$$

Here, ρ, t and $\mathbf{u}$ mean the density, time and velocity vector respectively. p and μ are the pressure and the molecular viscosity. ν_t is the sub-grid scale (SGS) eddy viscosity. x_k and $\mathbf{g}$ are the k-th coordinate the gravity vector. h, T, λ, Cp and Pr_t indicate the enthalpy, temperature, thermal conductivity, specific heat and turbulent Prandtl number respectively. F_L and Q_J are the Lorentz force and the Joule heat and are the interaction terms between the thermal hydraulics and the electromagnetic field. Overbar($\bar{\cdot}$) indicate the ensemble average of the SGS. With regard to the SGS eddy viscosity, the standard Smagorinsky model (Cs = 0.1) is applied in the present study.

In the following sections, the discrete manner and the coupling method are described.

Electromagnetic analysis model

The governing equations of electromagnetic field consist of Maxwell equations of electromagnetism and Ohm's law as:

$$\mathrm{rot}\,\mathbf{H} = \mathbf{j} + \frac{\partial \mathbf{D}}{\partial t}, \tag{4}$$

$$\mathrm{div}\,\mathbf{B} = 0, \tag{5}$$

$$\mathrm{rot}\,\mathbf{E} + \frac{\partial \mathbf{B}}{\partial t} = 0, \tag{6}$$

$$\mathbf{j} = \sigma\{\mathbf{E} + \mathbf{u} \otimes \mathbf{B} - \beta(\mathbf{j} \otimes \mathbf{B})\}. \tag{7}$$

Where, **H**, **j**, **D**, **B** and **E** are the Vector forms of magnetic field intensity, current density, electric flux density, magnetic flux density and electric field intensity, respectively. σ and β are the electric conductivity and the Hall constant. $\otimes$ indicates cross product. Then the Lorentz fore and the Joule heat are obtained in the following.

$$\mathbf{F}_L = \left(\frac{1}{\mu_m} \mathrm{rot}\,\mathbf{B} \right) \otimes \mathbf{B}\,, \tag{8}$$

$$Q_J = \frac{|\mathbf{j}|^2}{\sigma}\,. \tag{9}$$

Here μ_m is the magnetic permeability.

When electromagnetically isotropy and homogeneity are assumed in a tiny control volume, the magnetic flux is obtained as:

$$\mathbf{B} = \mu_m \mathbf{H}\,. \tag{10}$$

Furthermore, considering no displacement and electric convection currents, Eqs. (4) and (7) are reduced in the following.

$$\mathrm{rot}\,\mathbf{H} = \mathbf{j}\,, \tag{11}$$

$$\mathbf{j} = \sigma(\mathbf{E} + \mathbf{u} \otimes \mathbf{B})\,. \tag{12}$$

In general, the induction equation is obtained by substituting Eqs. (10)-(12) into Eq. (6) as:

$$\frac{\partial \mathbf{B}}{\partial t} = \mathrm{rot}(\mathbf{u} \times \mathbf{B}) + \frac{1}{\sigma \mu_m} \nabla^2 \mathbf{B}\,.$$

or (13)

$$\frac{\partial \mathbf{B}}{\partial t} + \nabla \cdot (\mathbf{u} \otimes \mathbf{B} - \mathbf{B} \otimes \mathbf{u}) = \frac{1}{\sigma \mu_m} \nabla^2 \mathbf{B}\,.$$

It is carefully noted that the solenoidal condition (Eq. (5)) is not a sufficient condition but a necessary condition for Eq. (13). Hence, an iterative solution is required when one solves Eq. (13) so as to satisfy the solenoidal condition at the same time.

Considering the coupling of electromagnetic field analysis with the LES thermal hydraulic computation, non-iterative manner is desirable for electromagnetic field analysis. Therefore, the vector finite volume method (VFVM) (Murashige, 2009), which is applied originally in an electromagnetic wave analysis and is extended to a finite volume method, is introduced in the present study.

In the VFVM, the electric field intensity (**E**) and the magnetic flux density (**B**) are solved separately. By substituting Eqs. (10) and (12) into Eq. (11), the electric field intensity is written as:

$$\mathbf{E} = \frac{1}{\sigma \mu_m} \mathrm{rot}\mathbf{B} - \mathbf{u} \otimes \mathbf{B} \tag{14}$$

With regard to the magnetic flux density, Eq. (6) is applied.

Figure 1 shows the arrangement of the definition point of the electric field intensity and the magnetic flux density in a control volume of computation. The magnetic flux density vector is located on the center of each surface (black arrow in Fig. 1), while the electric field intensity vector is defined at the center of each side (red arrow in Fig. 1). From Eq. (6), the magnetic flux density is decretized as:

$$\frac{\mathbf{B}^{n+1} - \mathbf{B}^n}{\Delta t} = -\mathrm{rot}\,\mathbf{E}\,, \tag{15}$$

here, superscript n and n+1 mean the current and the subsequent time step respectively. Multiplying the divergence operator ($\nabla \cdot$) into Eq. (15), one obtains the following equation.

$$\nabla \cdot \mathbf{B}^{n+1} - \nabla \cdot \mathbf{B}^n = -\Delta t \nabla \cdot (\mathrm{rot}\,\mathbf{E}) \tag{16}$$

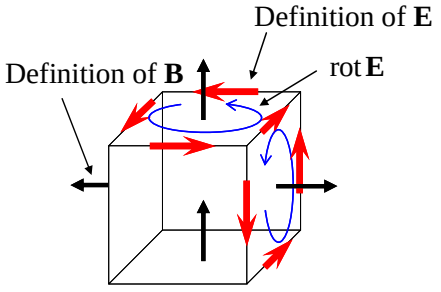

Fig. 1 Definition of E and B in control volume

When the staggered layout is applied as in Fig. 1, the electric field intensity vector is canceled each other during the divergence operation (see upper right side of control volume in Fig. 1). As a result, the right hand of Eq. (16) becomes null definitely in the computation. Hence, Eq. (16) is rewritten as:

$$\nabla \cdot \mathbf{B}^{n+1} = \nabla \cdot \mathbf{B}^n\,. \tag{17}$$

Thus the solenoidal condition (Eq. (5)) will satisfy automatically when it is achieved at the initial condition ($\nabla \cdot \mathbf{B}^{n=0} = 0$). Consequently, the magnetic field intensity can be updated non-iteratively.

In the analysis, the electric field intensity is calculated from Eq. (14) firstly based on the current (n) data set of **u** and **B**. Then the magnetic flux density is updated using Eq. (15). The Lorentz force and the Joule heat are obtained from Eqs. (8), (9) and (12).

Coupling method

In the LES computation, the second order Admas-Bashforth method and the second order central differential scheme are applied in the time marching term and the advective terms, respectively. Hence the Top-Hat filter is considered in ensemble average of the LES.

In the electromagnetic field analysis, the reciprocal product of the electric conductivity and the magnetic permeability behaves as a diffusive coefficient of the magnetic flux density as shown in Eq. (13). Liquid sodium has a low magnetic permeability (it is almost equivalent to the space permeability). As a result, the Courant-Friendrichs-Lewy (CFL) condition for the electromagnetic field becomes severer than that for the LES computation in the present study. Hence the fractional time step method is applied for the coupling.

In each time step of the computation, the electromagnetic field, the Lorentz force and the Joule heat is updated successively with the smaller time step in which the velocity field is kept to be constant. Then the temperature field is updated based on the time averaged Joule heat and the current velocity field. Lastly, the velocity field is updated based on the time averaged Lorentz force.

NUMERICAL STUDY OF THERMAL STRIPING PHENOMENON

In the numerical simulation of the thermal striping phenomenon, a T-junction of duct is assumed for simplicity and a magnetic field is embedded just after the junction. In the analyses, the influence of the Lorentz force on the statistic properties is investigated.

Analytical conditions

Figure 2 shows the geometry of the computation. The geometry consists of the main region and two drivers. The dimensions of the main and branch ducts are set to 40×40mm (D_m) and 12×12mm (D_b) respectively based on the water experiment (Nagao, 2004). The working fluid is liquid sodium and the Reynolds number (Re) of the main and branch ducts are set to 50,000 and 6,000 respectively where the working fluid from the branch duct flows along to the bottom side of the main duct. The temperature is set to 340ºC at the main flow and 430ºC at the branch flow.

A uniform magnetic field is embedded at the both of the top and bottom wall from $1D_b$ after the branch inlet to $3D_b$ as shown in Fig. 2. The Hartmann number (Ha) is set to 500 based on the main duct.

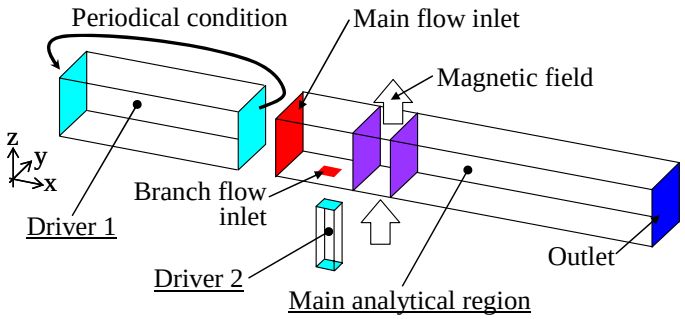

Fig. 2 Computational geometry

In the LES simulation, an inlet condition of fully developed turbulence is necessary for an accurate prediction. Hence, two drivers (driver1 and 2) are embedded aside from the main region as in Fig. 2. A periodical condition is assigned in each driver to achieve a fully developed turbulence. Then the inlet boundaries of the main region (red surface in Fig. 2) are coupled with the drivers. With regard to a boundary condition of energy, an isolated boundary is assumed in all walls for simplicity.

The computational domains are segmented into 210(x) ×56(y)×56(z) for the main region, 120×56×56 for the driver 1 and 20×20×40 for the driver 2. The mesh arrangement is indicated in Fig.3. As seen in Fig.3, the mesh adjacent to the wall has not a sufficient resolution to depict the viscous sub-layer. Morinishi and Kobayashi (1989) suggested that a reasonable prediction of turbulent channel flow had been achieved in a LES simulation by imposing a wall function model at wall boundary. Accordingly, the Spalding type wall function (Spalding, 1961) is introduced at the wall boundary in the present study so as to reduce a computational cost.

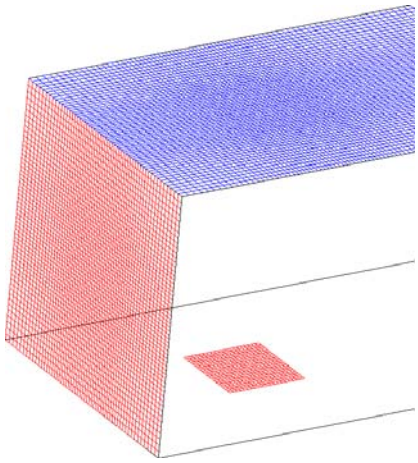

Fig. 3 Mesh arrangement (main region)

The time step for the thermal hydraulic simulation (Δt) is set to be achieved CFL = 0.1 automatically (approximately Δt = 1.0×10^{-4}s) and 1/50th of Δt is assigned for the electromagnetic field. In each analysis, a quasi steady state of turbulence has been computed firstly. Then statistical properties, such as an average and a root mean square of variables, are calculated during 2s of physical time. As concerns the magnetic permeability of liquid sodium, ten times as large as the space permeability is assigned considering an impurity of oxygen atom.

Result and discussion

Figures 4 and 5 show the instantaneous distributions of the normalized velocity magnitude divided by the average velocity of the main duct (U_m) and the temperature, respectively.

As concerns the velocity field, a large fluctuation is investigated when no magnetic field is embedded. It is also noted that a large stagnant region appears after the branch inlet (blue colored region). This is attributed to the fact that the upward flow from the branch duct acts as an obstacle. Furthermore, the large scale swell of the main flow is seen after the junction.

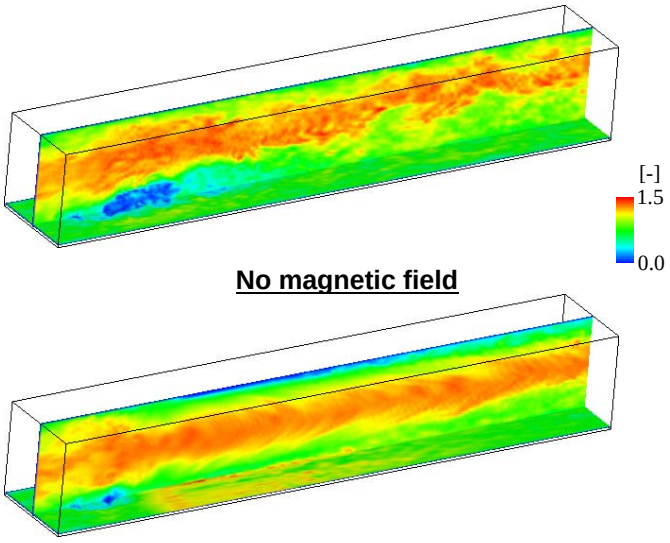

Fig. 4 Instantaneous velocity magnitude ($|\mathbf{u}|/U_m$) distribution

On the contrary, the fluctuation of the main flow decreases immediately from where the magnetic field is assigned in the magnetic field case. The stagnant region near the bottom wall almost diminishes and a comparative high velocity region is investigated near the bottom wall. Probably, the upward flow through the branch duct is stretched along to the streamwise and span wise directions due to Lorentz force. Since the main flow with less fluctuation is concentrated at the center and the low velocity region appears near the top side, it can be concluded that the main flow is forced to be laminarized.

With regard to the instantaneous temperature distribution, a large fluctuation is simulated in the no magnetic field case rather than that in the magnetic field case as shown in Fig. 5. At the same time, the high temperature region diminishes rapidly in case of the no magnetic field caused by the turbulent mixing.

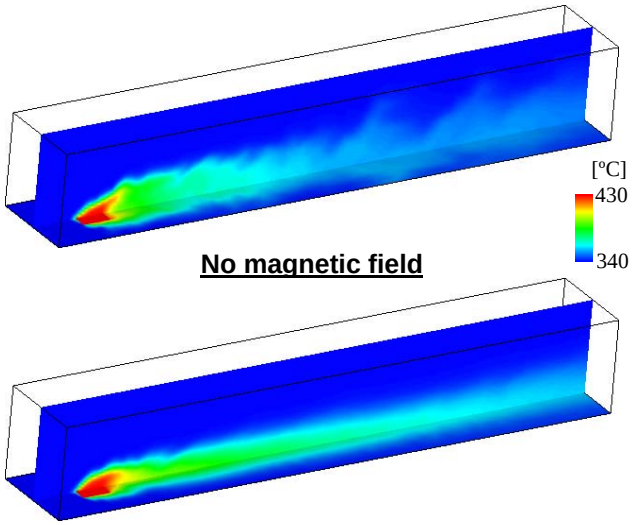

Fig. 5 Instantaneous temperature distribution

Figure 6 shows the distribution of (a) normalized average velocity magnitude and (b) normalized streamwise velocity fluctuation near the bottom wall. A solid box in the figure of the magnetic field case indicates the embedded magnetic field region at the wall.

As shown in Fig. 6(a), the large stagnant region appears in the no magnetic case same as mentioned in the instantaneous velocity result. When the magnetic field is embedded, the average stagnant region disappears immediately at the magnetic field area. Furthermore the high velocity region is generated at the center of the magnetic field area and vanishes gradually after the magnetic field area.

With regard to the fluctuation of the streamwise velocity, the most intense fluctuation appears just in front of the branch duct inlet. A local maximum exists in the downstream region which corresponds to the region where the stagnant region decreases. Hence it will be concluded that the local maximum of the velocity fluctuation comes from a large flow structure caused by the collision between the main and branch flows. Kamide et al. (2009) suggested in the experiment of tee piping with water that the frequency of the velocity fluctuation after the junction could be explained by the Strouhal number based on the diameter of the branch pipe. It is said that the present LES simulation follows the experimental observation.

When the magnetic field is embedded, the fluctuation vanishes quickly in the magnetic field area because of the Lorentz force. As seen in Fig. 6, a comparative high fluctuation exists where the high velocity region exists. As a

results a weak local maximum appears downstream the magnetic field area. After the region of the high fluctuation region, the magnitude becomes smaller than that of the no magnetic field case and the main duct inlet. This will be attributed to the fact that the main flow is laminarized due to the Lorentz force.

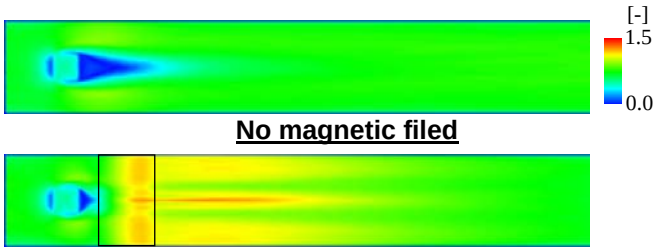

(a) Average velocity magnitude ($|\bar{\mathbf{u}}|/U_m$)

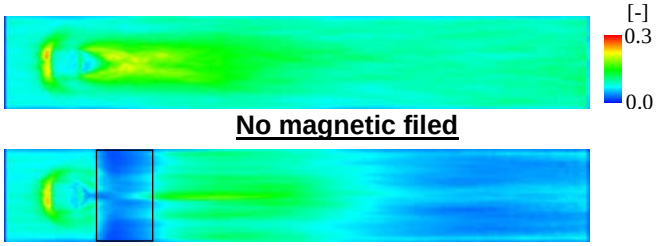

(b) Fluctuation of streamwise velocity (u'/U_m)

Fig. 6 Comparison of velocity distribution near bottom wall

The comparison of the normalized average temperature and the temperature fluctuation at the bottom wall is indicated in Fig. 7, where the temperature difference between the main and branch duct is applied for the normalization.

The average temperature decreases rapidly in case of the no magnetic field rather than that with the magnetic field due to turbulent mixing as in Fig. 7(a). It can be said that the embedding of the magnetic field has disadvantage from the view point of the circumferential thermal stress caused by a stationary temperature gradient.

As concerns the temperature fluctuation, the maximum fluctuation is investigated just in front of the branch inlet same as in the velocity fluctuation in both cases. However, unlike the velocity fluctuation, the local maximum appears the downstream area along to the side of the branch inlet. The energy mixing is initiated at the interface between the main and branch ducts. Consequently, the large fluctuation is investigated where the interface exists.

When the magnetic field is assigned, the temperature fluctuation decreases rapidly as seen in Fig. 7(b) because of the laminarization. Furthermore, it keeps a small magnitude even the velocity fluctuation increases after the magnetic field area (see Fig. 6(b)). Since liquid sodium is a low Prandtl number fluid (high thermal conductivity), a velocity fluctuation caused by a small scale turbulence has a less influence on the energy mixing.

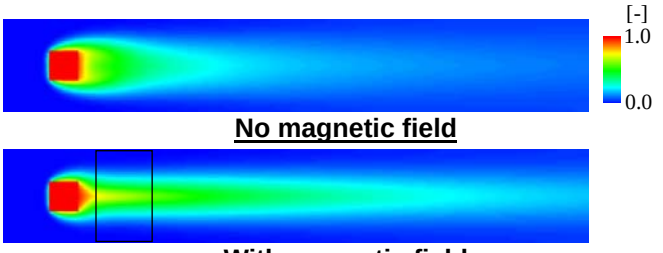

(a) Average temperature ($\bar{T}^*$)

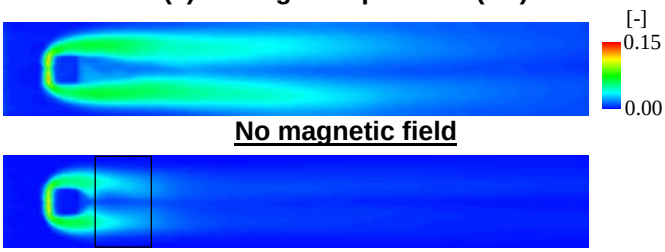

(b) Temperature fluctuation ($T'/\Delta T$)

Fig. 7 Comparison of temperature distribution at bottom wall

It is carefully noted that the thermal fatigue due to thermal striping phenomenon is much affected not by the stationary temperature gradient on the pipe but by the temperature fluctuation that leads to a temperature gradient in radial direction of pipe (Kasahara et al., 2002). When the magnetic field is embedded after the junction, the temperature fluctuation decreases significantly because of the main flow laminarization caused by the Lorentz force. Hence, it can be concluded that a passive control, which means that no additional device is implemented in the piping system, might be possible by using the Lorentz force although an effective manner should be considered to embed the magnetic field inside the piping system.

Figure 8 shows the vertical sectional view of magnetic density flux magnitude reduced by the boundary value at the center of the main duct. As seen in Fig. 8, almost no fluctuation is predicted in terms of the magnetic field because liquid sodium has a quite small magnetic permeability.

Fig. 8 Vertical sectional view of instantaneous magnetic density flux ($|\mathbf{B}|/B_b$) at center

CONCUSIONS

In a fast reactor (FR), liquid sodium is used as a coolant material. Since liquid sodium is invisible fluid, the authors have been developing a direct observation method by using

vacuum ultra violet (VUV) radiation. Liquid sodium is also an electromagnetic fluid and the Lorentz force will be induced and flow structure, ex. turbulent mixing, be influenced passively (without any additional devices) when magnetic field is embedded.

In the present paper, an applicability of the Lorentz force to fast reactor piping system has been numerically examined. For this purpose, the large eddy simulation (LES) coupled with an electromagnetic field analysis has been developed. A thermal fatigue problem, which will occurs after a pipe junction of different temperatures, is chosen as an example of the application using the Lorentz force. A junction of ducts is considered in the analysis for simplicity and a certain magnetic filed is assigned downstream the junction.

As a result of the numerical examination, it is demonstrated that the main duct flow is forced to be laminarized due to the Lorentz force and the velocity fluctuation that comes from the large flow structure due to the collision between the main duct and the branch duct flows is suppressed. Consequently, the temperature fluctuation decreases significantly when the flow goes through the magnetic field region. Hence it is concluded that a passive control might be possible by using the Lorentz force.

In a future work, the authors are planning to observe the influence of the Lorentz force on the flow structure directly by using the VUV radiation. Besides the measurement accuracy of the direct observation system will be examined comparing with the present simulation technique. It is also planned that an efficient embedding manner of magnetic field, such as a starting location, size of area and number of embedded magnetic field, will be investigated.

ACKNOWLEDGEMENT

Present study is the result of “Development of the Visualization Technology on Liquid Sodium Interface and flow in Fast Reactor System” entrusted to “Osaka University” by the Ministry of Education, Culture, Sports, Science and Technology of Japan (MEXT).

REFERENCES

Fukuda T. et al., 2010, Direct Observation and Control of Liquid Sodium Flow Dynamics Using VUV-LIF-PIV Technique under Lorentz Force, *Proc. of ICONE18*, Xi’an, China.

Kamide H. et al., 2009, Study on Mixing Behavior in a Piping and Numerical Analyses for Evaluation of Thermal Striping, *Nucl. Eng. and Design, 239, 58-67*.

Kasahara N., Takasho H. and Yacumpai A., 2002, Structural Response Function Approach for Evaluation of Thermal Striping Phenomena, *Nucl. Eng. and Design, 212, 281-292*.

Morinishi Y and Kobayashi T, 1989, A study on Wall Boundary Condition in LES, *Trans. of JSME, B, 55(511), 615-623* [in Japanese].

Murashige R, Yamaguchi A. and Takata T., 2009, Study on Numerical Analysis Method for Electromagnetic Fluid Using Vector Finite Volume Method Consistent with Solenoidal Condition, *Proc. of Nureth13*, N13P1331, Kanazawa, Japan.

Nagao A. et al., 2004, Study on Effects of Turbulence Promoter on Fluid mixing in T-junction Piping System, *JNC Technical report, JNC TY9400 2004-010* [in Japanese].

Spalding. D. B., 1961, A Single Formula for the Low of the Wall, *Trans. ASME, J. Appl. Mech., 28, 455-458*.